# Molecular-level understanding of highly selective heavy rare earth element uptake by organophosphorus modified MIL-101(Cr)

Keshavarz, Fatemeh; Kavun, Vitalii; van der Veen, Monique A.; Repo, Eveliina; Barbiellini, Bernardo

**DOI**
10.1016/j.cej.2022.135905

**Publication date**
2022

**Document Version**
Final published version

**Published in**
Chemical Engineering Journal

Chemical Engineering Journal 440 (2022) 135905

Contents lists available at ScienceDirect

Chemical Engineering Journal

journal homepage: www.elsevier.com/locate/cej

# Molecular-level understanding of highly selective heavy rare earth element uptake by organophosphorus modified MIL-101(Cr)

Fatemeh Keshavarz [a,*], Vitalii Kavun [b], Monique A. van der Veen [c], Eveliina Repo [b], Bernardo Barbiellini [a,d]

[a] Department of Physics, LUT University, Yliopistonkatu 34, FI-53850 Lappeenranta, Finland
[b] Department of Separation Science, LUT University, Yliopistonkatu 34, FI-53850 Lappeenranta, Finland
[c] Catalysis Engineering, Department of Chemical Engineering, Delft University of Technology, Van der Maasweg 9, 2629 HZ Delft, The Netherlands
[d] Department of Physics, Northeastern University, Boston, MA 02115, USA

ARTICLE INFO

*Keywords:*
Metal-organic frameworks
Rare earth elements
Selectivity
First-principles calculations
Water treatment

ABSTRACT

Selective separation of rare earth elements (REEs) from solutions of mixed heavy and light metals by solid adsorbents is an important challenge in the fields of water treatment and metal recovery. The main challenge is water instability of many adsorbents, specifically metal–organic frameworks (MOFs), and their low selectivity. Grafting particular organophosphorus compounds (OPCs) on the MIL-101(Cr) MOF can provide both stability and selectivity. When the tributyl phosphate (TBP), bis(2-ethylhexyl) hydrogen phosphate (D2EHPA or HDEHP) and bis(2,4,4-trimethylpentyl) phosphinic acid (Cyanex®-272) OPCs are grafted and applied to mixed-metal aqueous solutions containing $Co^{2+}$, $Ni^{2+}$, $Cu^{2+}$, $Zn^{2+}$, $Nd^{3+}$, $Gd^{3+}$ and $Er^{3+}$, MIL-101(Cr) offers high selectivity towards the $Nd^{3+}$, $Gd^{3+}$ and $Er^{3+}$ REEs (with stronger affinity towards $Er^{3+}$). However, the underlying chemistry is unknown and the factors leading to the selectivity remain poorly understood. To uncover the key molecular-level factors, we performed state-of-the-art computational simulations using a combination of high-level density functional theory (DFT), semi-empirical calculations, and configurational sampling of the metal ion-MOF binding modes in aqueous solutions. Our simulation study reproduced the available experimental results, in addition to determining the contributing intermolecular interactions, uptake modes and the most significant structural features for improving selectivity towards the REEs. Therefore, our most important result is rationalization of the mechanism of REE separation by OPC-grafted MOFs using quantum mechanical and electrostatic principles. The results provide guidelines for synthesis of OPC-grafted MIL-101(Cr) structures with enhanced selectivity and stability. Moreover, an efficient computational framework is proposed to facilitate comprehensive modeling of similar systems.

## 1. Introduction

The field of selective recovery of rare earth elements (REEs) is intensively developing because REEs are highly demanded in the production of high-tech devices and their recovery is an essential step in the transition towards green technologies. Several techniques are available to recover REE from concentrated solutions. However, their performance declines rapidly with the reduction of REE concentration. The reason is their high sensitivity to acidic conditions, the necessity of acid consumption in large amounts and considerable REE loss [1]. Therefore, it is required to develop feasible alternative techniques.

An alternative option is the use of solid adsorbents, such as metal–organic frameworks (MOFs). As highly crystalline porous materials, MOFs can provide an intriguing platform to develop an adsorbent material for specific purposes. They can be synthesized by following the principles of reticular chemistry and forming strong bonds between metallic clusters and charged organic linkers [2]. Because of the flexible choice of their structural components, highly diverse MOFs with large surface areas can be prepared and chemically modified to adjust their physiochemical properties for a wide range of applications, including adsorptive water treatment [3]. Despite such advantages, poor water-resistance of most MOFs is significantly hindering their applications in

* Corresponding author.
*E-mail addresses:* fatemeh.keshavarz@lut.fi (F. Keshavarz), vitalii.kavun@lut.fi (V. Kavun), m.a.vanderveen@tudelft.nl (M.A. van der Veen), eveliina.repo@lut.fi (E. Repo), bernardo.barbiellini@lut.fi (B. Barbiellini).

https://doi.org/10.1016/j.cej.2022.135905
Received 20 January 2022; Received in revised form 7 March 2022; Accepted 16 March 2022
Available online 19 March 2022

aqueous environments. However, better water stability can be obtained with the MOFs composed of high-valent metal cations and carboxylate linkers [4–6], such as MIL-101(Cr).

MIL-101(Cr) is a highly water-resistant MOF that has found many aqueous-phase applications, such as drugs delivery [7], water treatment [8], and adsorption and selective recovery of desired metals [9]. It possesses a large specific surface area (ca. 3300 $m^2\ g^{-1}$) and pore volume (1.8 $cm^3\ g^{-1}$), and its coordinatively unsaturated metal sites can be post-synthetically modified to enhance its properties [10]. However, the use of any solid adsorbent (including MIL-101(Cr)) in selective REE recovery would be quite challenging because of the presence of competing multivalent ions in aqueous solutions [11]. Particularly, lanthanides present similar physicochemical properties and ligand affinities. Therefore, their separation is mainly driven by the difference in their ionic radii, making their selective separation more complicated [12]. The challenge can be overcome by grafting phosphorous-containing functional groups, specifically organophosphorus compounds (OPCs), onto the adsorbents.

OPCs such as tributyl phosphate (TBP), bis(2-ethylhexyl) hydrogen phosphate (D2EHPA or HDEHP) and bis(2,4,4-trimethylpentyl) phosphinic acid (Cyanex®-272) have shown promising efficiency in liquid–liquid extraction and the separation of REEs [11,13]. HDEHP preferentially forms complexes with the heavier REEs of organic phases. Consequently, it has been successfully utilized for selective separation of light (LREE; La-Sm) and heavy (HREE; Eu-Lu) REEs [14]. Cyanex-272 typically shows a poorer separation efficiency within the lanthanide series (relative to HDEHP), but it demonstrates high affinity towards HREEs [1,14]. The neutral TBP extractant has been successfully applied to recovery of REEs from different solutions, but its extraction performance is mainly limited to LREEs. The efficiency of TBP in separation of HREEs decreases drastically with an increase in atomic number [14,15].

Unfortunately, few studies (e.g. [16–19]) have evaluated the adsorption efficiency of OPC-grafted solid adsorbents. Our earlier experimental study on TBP-modified MIL-101(Cr) (MIL-101-T50), HDEHP-modified MIL-101(Cr) (MIL-101-H50) and Cyanex®-272-modified MIL-101(Cr) (MIL-101-C50) [10] demonstrated the efficient and intriguing performance of OPC-grafted MOFs for selective separation of heavy REEs from mixed solutions of light and heavy elements. For instance, MIL-101-T50 showed 100% and 95% selectivity towards $Er^{3+}$ in the presence of transition metal ions ($Co^{2+}$, $Ni^{2+}$, $Cu^{2+}$ and $Zn^{2+}$) and light rare earth ions ($Nd^{3+}$ and $Gd^{3+}$), at pH 5.5. Though the overall adsorption efficiency of the modified MOFs increased in the order of TBP < Cyanex-272 < HDEHP, the selectivity towards $Er^{3+}$ followed the Cyanex-272 < HDEHP < TBP trend. Moreover, the functionalized MOFs were found to be highly competitive compared to many other synthetic materials (such as commercial phosphorous ion-exchange resins [20], zirconium organophosphonates [21,22], some other modified MOFs [23–25], and porous silica and cellulose based materials with amino and carboxyl functional groups [26,27]), especially at acidic and neutral pH conditions [28]. Despite such motivating experimental observations, the mechanisms underlying the highly selective $Er^{3+}$ adsorption process and the difference between the performance of the three OPCs remains unknown.

The question we would like to answer is: what causes the success of OPC-grafted MIL-101(Cr) in selective separation of REEs? To answer this question, we need to understand the separation process at the molecular level. To date, few investigations have focused on the relationship between the chemical structure of ligands and their extraction efficiency. Some extensive experimental studies [29,30] have demonstrated the significance of the chelating angle of the functional groups on selective coordination with REEs. Another study has shown the effect of the length and branching of neutral OPC alkyl chains on metal extraction efficiency [31]. Some theoretical studies have revealed the complexation mechanism between some OPCs and REEs in liquid–liquid extraction processes [32,33]. However, there is no theoretical study regarding the mechanism of REE separation by OPC-grafted adsorbents and, particularly, MOFs. Also, the general mechanism ruling the selectivity of adsorbents towards REEs remains poorly understood.

To uncover the molecular interactions and parameters involved in the success of OPC-modified MIL-101(Cr) and guide further studies towards the best selection of ligands for MOF functionalization, we employ a novel, simple and efficient modeling framework based on first principles calculations. First, we explain the simulation method in detail. Then, we use the modelling results in parallel with the summarized experimental data to discuss: 1) the effect of MOF functionalization (OPC grafting) on the available surface area, 2) the interactions involved in the process of MOF functionalization by the OPCs and solvent effect, and 3) the molecular keys to selective uptake of the REEs by MOFs. In our conclusion, we provide a summary of the most important findings.

## 2. Modeling details

Modeling of REE recovery was broken into several steps to simplify the modelling process. First, the computational parameters regarding the MOF model were optimized by identifying its ground state and evaluating the performance of different density functional theory (DFT)-based computational levels. Then, the OPCs were *manually* added to the MOF model in several configurations to simulate modification of MIL-101(Cr) by the OPCs. The modification process was modeled in different phases to study solvent effect on the synthesis process. To evaluate the effect of model size and the presence of the MOF's organic ligands on our results, we also studied OPC addition to a larger MOF model containing several phenyl-containing ligands. After observing insignificant effect of the ligands on OPC adsorption, we used the simpler (phenyl-free) MOF model for the metal recovery simulations. To simulate metal recovery, we deployed a systematic *configurational sampling* technique and added a number of water molecules, nitrate anions and the metal ions to the OPC-modified MOF structures. Full details are as follows.

### 2.1. Modeling of MIL-101(Cr) and its modification by OPCs

All electronic structure calculations were carried out in the framework of DFT by Gaussian 16 revision A.03 [34]. Since the unit cell of MIL-101(Cr) is composed of over 10 000 atoms, the synthesized MOF was modelled by focusing on its secondary building unit (SBU), using the

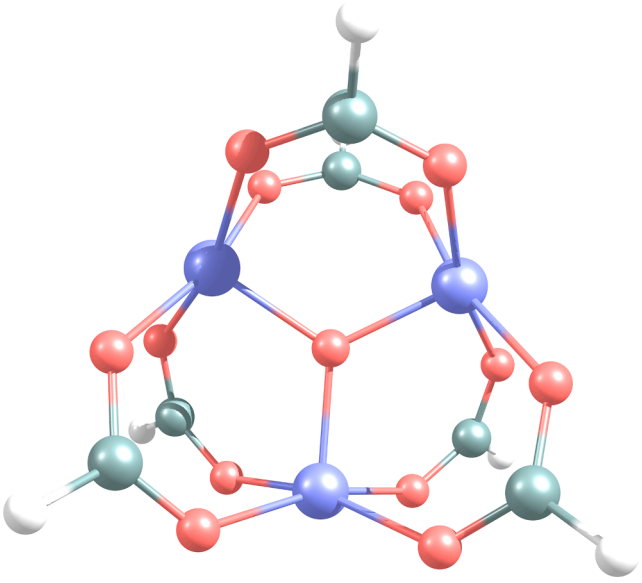

**Fig. 1.** The selected MIL-101(Cr) model. The purple, red, grey, and white balls represent the Cr, O, C and H atoms, respectively.

$[M_3O(OOCR)_6L_3]_n^+$ paddlewheel complex (M = Cr, R = H, n = 1, no L ligand) shown in Fig. 1. The model with and without water or axial anions has been successfully adopted by many studies [35–39]. However, the studies have considered various spin states for their adopted models. For example, Hu et al. [37] concerned the singlet state (neutral anion-free model) while de Oliveira et al. [36] and Mavrandonakis et al. [35] respectively modeled it in the quartet and dectet states (+1 charge for the anion free model). In the present study, the singlet neutral model was used as a starting point. Then, as one Cr(III) site can be occupied by an anion, the + 1 charge state was also studied. At this charge state, the Cr(III) sites prefer antiparallel spin alignment of their $d^3$ orbitals [36], which results in ferromagnetic properties [35,40]. Therefore, all possible spin states from low spin (doublet) to high spin (dectet) were evaluated. After optimization of the model's geometry at all charge-spin states, and assessment of their structural stability (through harmonic frequency calculations), geometry symmetry breaking, spin contamination and energy profiles, we chose the dectet state as the ground state. The details are reported in Section S1 of the Supplementary data (Figs. S1-S3 and Tables S1 and S2). Notably, to minimize the spin-contamination and symmetry breaking issues, the singlet-state calculations were performed using a restricted wavefunction formalism [41] while the spin of the doublet to dectet open-shell systems were treated as unrestricted [42,43].

For the preliminary calculations, multiple density functionals were tested to find the optimal computational level. For this purpose, the methods commonly used for MOF modeling (and specifically for MIL-101) were screened, including the B3LYP [44], M06-2X [45], M06-L [45], PBE [46], PW91 [47], and ωB97XD [48] methods, which have been respectively used in for example refs. [37] and [49], [38], [38 and 39], [50–54,54], and [55]. To include dispersion effects and increase the accuracy of van der Waals interaction description, the Grimme's D3 (GD3) semi-empirical dispersion correction [56] was applied to all methods, except PW91 and ωB97xD. In the case of ωB97xD, the functional originally supports dispersion treatment by including a long-range exchange–correlation correction [48]. However, the PW91 does not inherently support dispersion interaction, and the required parameters are not implemented in the Gaussian package. First, all methods were coupled with the def2-TZVP basis set [57,58], which can provide both accuracy and affordable computational cost [59]. Then, the optimal method was chosen by evaluating the performance of several basis sets with respect to the available experimental data. Section S2 and Table S3 report the corresponding results and outline M06-L/def2-TZVP as the optimal level.

After optimization of all modeling parameters, the TBP, HDEHP and Cyanex-272 (hereafter mentioned as Cyanex for simplicity) molecules (see Fig. S4 for their 2D structures) were optimized at the M06-L/def2-TZVP level. The optimized geometries of the OPCs (shown in Fig. S4) were manually added to the geometry-optimized MIL-101(Cr) model in several configurational states. Because of the fact that the addition of the OPC molecules to the MOF involves direct interaction of the phosphate and phosphinic groups of the OPCs with the $Cr^{3+}$ metals of the MOF model, we assumed that the conformational changes of the OPCs' alkyl groups would not alter the OPC-MOF adsorption energies, significantly. This was later supported by observing insignificant interaction between the MOF's organic ligands and the OPCs' alkyl groups (see the "OPC/MIL-101(Cr) interaction" sub-section). Consequently, we considered just one conformational state for each OPC. The OPC/MIL-101(Cr) structures were relaxed (optimized) at the dectet spin state to permit the OPCs adjust their conformational state relative to the MOF model. The calculations were carried out in gas phase, and in the toluene and water solvents to evaluate solvent effect on the functionalization process. The toluene and water solvents were simulated implicitly using the SMD polarizable continuum model [60]. Throughout the calculations, the stability of all structures was verified by the absence of any imaginary frequencies using harmonic frequency calculations. In the end, we added a few phenyl-containing ligands to the most favorable HDEHP/MOF model configuration (as a sample) in toluene (i.e., the HDEHP-b configuration) to assess the effect of linkers on OPC interaction. The intermolecular interactions were extracted from natural bond-orbital (NBO) analysis.

### 2.2. Modeling of metal recovery by the modified MOFs

Adsorption of the $M^{n+}$ ions by OPC-grafted MIL-101(Cr) was modeled on the basis of the configurational sampling method developed by Kubečka et al. [61]. This method has been successful in reproducing and explaining experimental observations in our earlier studies [62–64] and predicting the global minimum (GM) structure of water-phase molecular complexes [65,66]. Single-point energy calculations (at the M06-L/def2-TZVP level) on the metal ions showed that $Co^{2+}$, $Cu^{2+}$, $Er^{3+}$, $Gd^{3+}$, $Nd^{3+}$, $Ni^{2+}$ and $Zn^{2+}$ are respectively at their quartet, doublet, doublet, doublet, sextet, triplet and singlet spin states in aqueous solutions. When complexed with the modified MOF (with dectet spin state), the overall spin state of the system would change, requiring careful spin state analysis. In addition, the large size of the system makes the computations more demanding. Therefore, the configurational sampling of Kubečka et al. [61] was modified as follows.

For each $M^{n+}$/MOF complex, all possible high to low spin states were considered. Among the OPC/MIL-101 models, the most favorable water-phase configurations (Cyanex-b, HDEHP-b and TBP-b) were selected. As previous experimental and theoretical studies have indicated coordination of the lanthanides to three nitrate ions in aqueous nitrate solutions in the presence of organic ligands [32,67], several nitrate ions were considered to neutralize the modeled systems. Then, the artificial bee colony (ABC) algorithm (the ABCluster 1.4 program [68,69]) was employed to find 500 local minima (LM) structures for each $M^{n+}$/MOF/nitrate complex at each possible spin state through generation of 800 initial guesses. The initial structural guesses were improved in 250 generation rounds using 4 scout bees. Throughout the calculations, the generated LM structures were evaluated and sorted based on their energy. The energy was calculated as the sum of Lennard-Jones (LJ) and Columbic interactions. For Columbic interactions, atomic polar tensor (APT) charges resulted from water-phase M06-L/def2-TZVP calculations were used. For LJ interactions, the LJ parameters for description of the MIL-101(Cr) model, the OPCs, the REEs, and the divalent metal ions (and also nitrate anion) were respectively extracted from the studies of Bernini et al. (UFF) [70], Das and Musharaf Ali (OPLS-AA) [71], Migliorati et al. (OPLS-AA) [72] and Li and Merz (OPLS-AA) [73]. Then, the LM structures were imported to the XTB 6.0.1 [74] program and geometry optimized using the GFN2-xTB [75] spin-restricted semi-empirical method, in gas phase. Next, the redundant (non-unique) structures were filtered out and the calculation was repeated using the analytical linearized Poisson-Boltzmann (ALPB) implicit water model [76,77]. Notably, the XTB program does not support SMD solvent calculations. For each complex and at each spin state, the structure with the lowest electronic energy was selected as the GM structure. Then, the GM structures of each complex resulting from various spin states were compared and the one having the lowest electronic energy was selected as the ground state structure. When the energy difference between two spin states was below 100 kJ $mol^{-1}$, both spin states were kept for further calculations.

After identification of the ground spin state of each complex, the outlined process was repeated by adding several explicit water molecules to the systems. The number of the water molecules was a compromise between chemical-soundness and computational feasibility. We started with 50 water molecules. However, the large system size and calculation expenses did not permit the generation of the LM structures to proceed. Therefore, we tried reducing the number of water molecules gradually until the LM structure generation process completed. Importantly, we did not apply any time limit for any of the calculations. We ended up with 6 explicit water molecules for each system and repeating the configurational sampling approach from the

initial LM generation step. The TIP3P model [73] was used to describe the LJ parameters of the explicit water molecules. After gas and solvent phase calculations by the XTB program, the LM structures were filtered again to limit the calculations to the unique structures. Then, frequency calculations were performed in the water phase and the GM structures were indicated by the lowest Gibbs free energy values. DFT calculations were skipped because of the high computational cost and the satisfying GFN2-xTB results.

## 3. Results and discussion

### 3.1. Effect of OPC grafting on surface area

In experimental BET surface area measurements [10], we observed the decrease of surface area with successive increase of OPC dosage (see Fig. S5). For example, we detected about 81% decrease in the surface area of MIL-101(Cr) when the amount of Cyanex was increased from 5 wt% to 100 wt%. The change can be attributed to partial filling/blockage of the MOF pores by the grafted OPCs as they are spatially hindering with their relatively long alkyl chains (see Fig. S4). According to our computational estimations on "single molecules" in gas phase, free Cyanex, HDEHP and TBP respectively occupy 237.66, 242.99 and 245.46 $cm^3\ mol^{-1}$ space. When they are adsorbed onto the "MOF model" (235.53 $cm^3\ mol^{-1}$) in the configurational modes shown in Fig. S6, the average molar volumes of the generated OPC-MOF models would be respectively 451.40, 398.16 and 370.97 $cm^3\ mol^{-1}$. This reflects 57–92% increase in the volume of the "MOF model" upon addition of each single OPC molecule and implies a decrease in the total pore volume of MIL-101(Cr) upon MOF modification by the OPCs. Though free Cyanex is smaller than HDEHP and TBP, it fills up the MOF pores more significantly (91.65% increase in the MOF model's volume vs. 69.05% for HDEHP and 57.50% for TBP). This is consistent with the BET results [10], showing a decrease in specific surface area (and total pore volume) from 3341 $m^2\ g^{-1}$ (1.80 $cm^3\ g^{-1}$) for pristine MIL-101(Cr) to 442 $m^2\ g^{-1}$ (0.19 $cm^3\ g^{-1}$; 89% reduction), 1028 $m^2\ g^{-1}$ (0.47 $cm^3\ g^{-1}$; 74% reduction) and 1158 $m^2\ g^{-1}$ (0.57 $cm^3\ g^{-1}$; 68% reduction) for the MOF loaded with 50 wt% Cyanex, HDEHP and TBP compounds, respectively. The reason behind these changes can be related to the spatial orientation of the OPCs inside the MOF pores. According to Fig. S6, capping of the MOF's SBU by the OPCs adds a large volume inside the MOF pores. The alkyl groups of the OPCs tend to spread over the MOF sites or point outwards from the metal centers, blocking the SBU and reducing the accessible MOF surface area.

### 3.2. OPC/MIL-101(Cr) interaction

In our experimental study [10], MIL-101(Cr) was post-synthetically modified with OPCs in toluene. The solid materials were subsequently characterized in the gas phase and used for aqueous phase metal recovery. Therefore, we modelled the functionalized MOFs in all these phases. Notably, optimization of the OPC-free MIL-101(Cr) model (shown in Fig. 1) did not converge completely in the toluene and water phases by being trapped in an inevitable convergence loop that could not be avoided by changing the optimization criteria (such as solvent model). To be more specific, the default convergence criteria included $4.50 \times 10^{-4}$ Hartree $Bohr^{-1}$ for maximum force, $3.00 \times 10^{-4}$ Hartree $Bohr^{-1}$ for RMS force, $1.80 \times 10^{-3}$ Å for maximum displacement and $1.20 \times 10^{-3}$ Å for RMS displacement. In the cases of the OPC-free model in toluene and water, the three RMS force, maximum displacement, and RMS displacement convergence criteria were met, but the change in maximum force did not go lower than $1.15 \times 10^{-3}$ Hartree $Bohr^{-1}$. The adsorption energies for each system were calculated as the energy change resulted from the addition of the two OPC and MOF model components to each other, meaning that the adsorption energies were relative energies calculated with reference to the energy of the OPC-free MOF model at the associated phase. For example, the adsorption Gibbs free energies ($\Delta G$) were calculated as the difference between the Gibbs free energy of the OPC-modified MOF model ($G_{OPC\text{-}MOF}$) and the Gibbs free energy of the two OPC ($G_{OPC}$) and MOF model ($G_{MOF}$) components; $\Delta G = G_{OPC\text{-}MOF} - G_{OPC} - G_{MOF}$. Therefore, we expect the adsorption energy results of every phase to be qualitatively valid regardless of quantitative accuracy.

Table S4 reports thermodynamics of MOF modification by OPC in toluene, and Table S5 and Fig. 2 summarize the Gibbs free energy of OPC adsorption on MIL-101(Cr) in the three phases. Based on Table S5 and Fig. 2, the presence of the toluene and water solvents weakens the interaction of the OPCs with the MOF. Particularly, aqueous solutions weaken OPC interaction dramatically, and decrease TBP's average adsorption Gibbs free energy from −151.1 to −6.9 kJ $mol^{-1}$ (see Table S5). Regardless of the solvent phase, Cyanex and then HDEHP adsorb more strongly on the SBU and TBP establishes a weaker link. This explains the higher loading of HDEHP onto the MOF compared to TBP loading (1.15 mmol $g^{-1}$ vs. 1.03 mmol $g^{-1}$ for MIL-101-T50) observed by thermogravimetric analysis (TGA) [10]. Notably, Cyanex loading could not be measured through TGA because of its continuous degradation [10]. Moreover, the obtained order of OPC adsorption Gibbs free energies implies higher stability of Cyanex (MIL-101-C50) and HDEHP-grafted MIL-101(Cr) (MIL-101-H50) relative to the TBP-modified MOF. This is in line with the amounts of leached chromium from the modified MOFs traced by ICP-MS (pH 1–6) and that of phosphorous at pH 5.75, in our experimental work [10].

The effect of the MIL-101(Cr) ligands on OPC adsorption was evaluated by adding a few phenyl-containing ligands to the HDEHP-b configuration (as a sample structure). The optimized structure and the associated adsorption energies are shown in Fig. 3. As seen, the phenyl-containing ligands increase the electronic energy ($\Delta E$), potential energy ($\Delta U$) and enthalpy ($\Delta H$) of OPC adsorption, negligibly. But they lower the entropy ($\Delta S$) relatively significantly. Nevertheless, the entropy changes neutralize the increase of enthalpy, giving slightly less

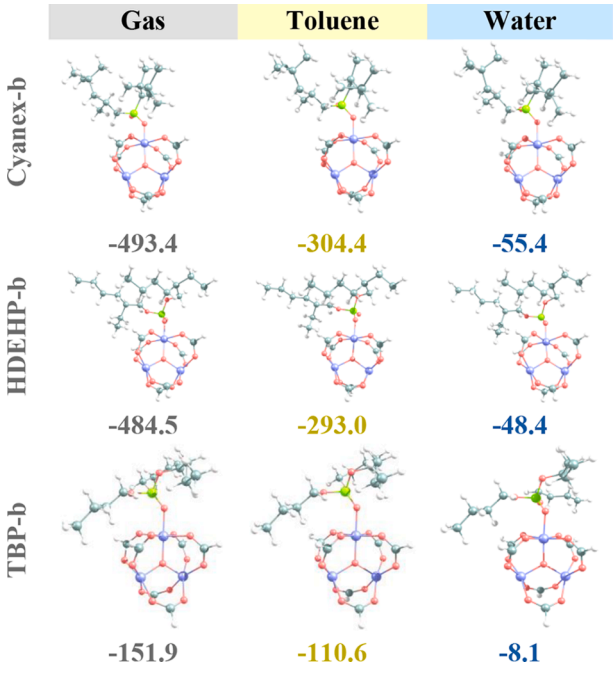


**Fig. 2.** Sample geometries of the OPC-grafted MIL-101(Cr) models optimized in the gas, toluene, and water phases. The values reported under each structure are the corresponding adsorption Gibbs free energies at 1 atm and 298.15 K, in kJ $mol^{-1}$. The purple, green, red, grey, and white balls respectively represent the Cr, P, O, C and H atoms. See Fig. S6 and Table S5 for the structures and adsorption Gibbs free energies of the other OPC/MIL-101(Cr) model configurations.

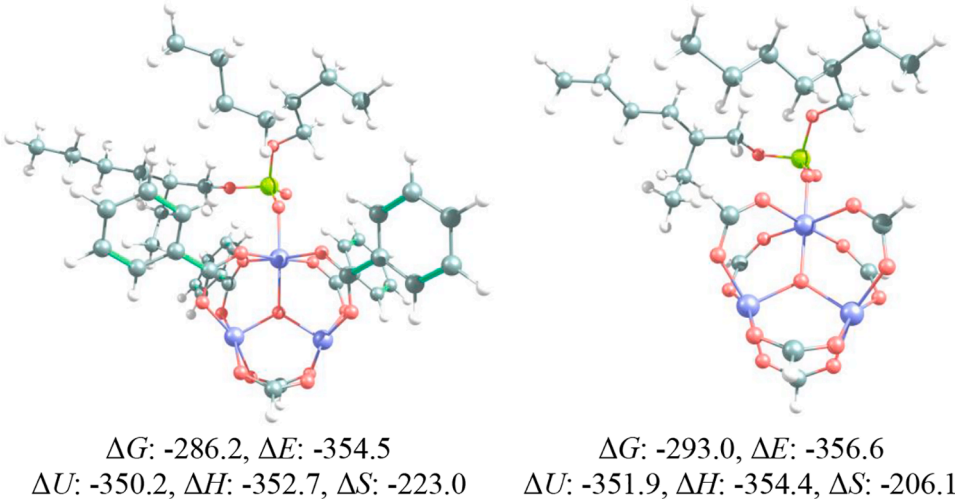


**Fig. 3.** Geometries and adsorption energies of HDEHP adsorption on the phenyl-containing and phenyl-free MIL-101(Cr) models. The purple, green, red, grey, and white balls respectively represent the Cr, P, O, C and H atoms. The values of ZPE-corrected electronic energy ($\Delta E$), potential energy ($\Delta U$), enthalpy ($\Delta H$) and Gibbs free energy ($\Delta G$) of OPC adsorption are in kJ mol$^{-1}$, while the adsorption entropy ($\Delta S$) values are in J mol$^{-1}$.

favorable adsorption ($\Delta G = \Delta H - T\Delta S$; $T$: temperature). In real MOF structures, the phenyl groups would be fixed in place, leading to a rigid structure. This can limit the changes in entropy (compared to the modeled structure), decreasing Gibbs free energy of adsorption. However, the net changes in $\Delta G$ should not be considerable.

To gain insight into the differences between the interaction of the three OPCs and the observed solvent and ligand effects, NBO analysis was performed on the most favorable OPC/MIL-101(Cr) adsorption modes in toluene (i.e., the Cyanex-a, HDEHP-b and TBP-b configurations), and the phenyl-containing HDEHP-b structure. Table S6 summarizes the most significant charge transfers between the OPCs and the MOF model. In this table, the higher the stabilization energy ($E^{(2)}$), the stronger the charge transfer and the corresponding interaction. Therefore, the main interactions responsible for adsorption of the OPCs onto the MIL-101(Cr) structure refer to charge transfer from the lone pair (LP, nonbonding) orbital of the OPCs' oxygen atoms to the anti-nonbonding (LP*) orbital of Cr ($LP(O_{Cr})_{OPC} \rightarrow LP^*(Cr)_{SBU}$). There are four other types of charge transfer important in the adsorption process: 1 and 2) from the bonding (σ) and anti-bonding (σ*) orbitals formed between the Cr-binding OPC oxygen atom and the phosphorous atom of OPC to the LP* orbital of Cr ($\sigma(PO_{Cr})_{OPC} \rightarrow LP^*(Cr)_{SBU}$ and $\sigma^*(PO_{Cr})_{OPC} \rightarrow LP^*(Cr)_{SBU}$), 3) from the core (CR) orbital of the OPC's Cr-bound oxygen to the LP* orbital of Cr ($CR(O_{Cr})_{OPC} \rightarrow LP^*(Cr)_{SBU}$), and 4) from LP of the Cr-bound oxygen atom in OPC to the σ* orbital formed between Cr and the bridging oxygen ($O_\mu$) of the SBU ($LP(O_{Cr})_{OPC} \rightarrow \sigma^*(CrO_\mu)_{SBU}$). In other words, the main interaction controlling the MOF modification process by OPCs is Cr interaction with the alkyl-free oxygen atom of OPC. This does not mean that the interactions of the other molecular moieties have zero effect on the adsorption reaction, but their effects appear mostly as dispersion interaction with stabilization energies below 25 kJ mol$^{-1}$. This statement is extendable to the full MIL-101(Cr) structure because the NBO results of the HDEHP-b structure with several phenyl-containing ligands did not highlight any significant interaction between HDEHP and the phenyl-containing ligands.

Furthermore, Table S6 indicates that the stability of the OPC-modified MIL-101(Cr) structures depends on the net stabilization energy resulted from the established charge transfer processes. For TBP, alkylation of three oxygen atoms leaves it with just one oxygen atom for binding to the Cr atom of SBU, which carries less negative charge (-0.971693 e) compared to HDEHP (-1.087378 and −1.069565 e) and Cyanex (-1.125101 and −1.152260 e), in its MOF-free state (toluene phase; APT charge). Accumulation of a lower level of negative charge on TBP's free oxygen weakens its ability of effective electrostatic interaction with the positively charged Cr atom. Consequently, TBP establishes charge transfer processes (interactions) like those of HDEHP and Cyanex, but the stabilization energies are lower in value. This implies that application of OPCs with more negative charge localized on their alkyl-free oxygens can give more stable OPC-modified MOF structures, and the chemistry of the OPCs' alkyl groups just matters with respect to their role in re-distribution of charge in their phosphate group.

According to the NBO results, we expect any environmental factor influencing the strength of the O-Cr bond between the OPCs and SBU to alter stability of the synthesized MOFs. The observed solvent effect roots in the hydrophobicity of the OPCs' alkyl chains and hydrophilicity of their phosphate groups, both facilitating OPC interaction with the solvent molecules and weakening their interaction with the SBU. Particularly, hydrogen bonding between water molecules and the SBU-bound oxygen of TBP can weaken the O-Cr bond, leading to weakened adsorption and the lower structural stability of TBP-modified MIL-101 (Cr) (MIL-101-T50) in aqueous solutions. Similarly, low pH levels can lead to the protonation of the most negatively charged OPC oxygen atom (the one linked to the SBU for TBP and the free O atom for HDEHP and Cyanex), weakening the OPC-SBU O-Cr bond and destabilizing the modified structures.

### 3.3. Metal adsorption by OPC-modified MIL-101(Cr)

The first step in modelling of metal ion recovery from aqueous solutions by the OPC-modified MOFs was determining the systems' spin states. As aforementioned, the OPC-modified MOF model is dectet and each metal ion exists in its unique spin state. After evaluating all possible spin states, the ground spin state of every MOF-metal ion system was indicated and reported in Table S7. According to our evaluations, every system tended to be more stable at the lowest spin state combination. After spin state determination, the global minimum metal ion-MOF-nitrate-water complexes were identified (shown in Fig. 4) and thermodynamics of metal recovery was analysed. In the analyses, it was considered that larger difference in the Gibbs free energy of complex formation in the presence of a specific metal ion reflects higher selectivity towards that ion. The average complexation Gibbs free energies were calculated as $\Delta G_{cmx,avg} = (G_{tot} - \sum_i n_i G_i)/m$; with $\Delta G_{cmx,avg}$, $G_{tot}$, $G_i$, $n$ and $m$ being the average complexation Gibbs free energy, the total Gibbs free energy of the system containing all components, the Gibbs free energy of isolated component $i$, the total number of component $i$ present in the system, and the total number of ionic and molecular species in the system, respectively. The average complexation Gibbs free

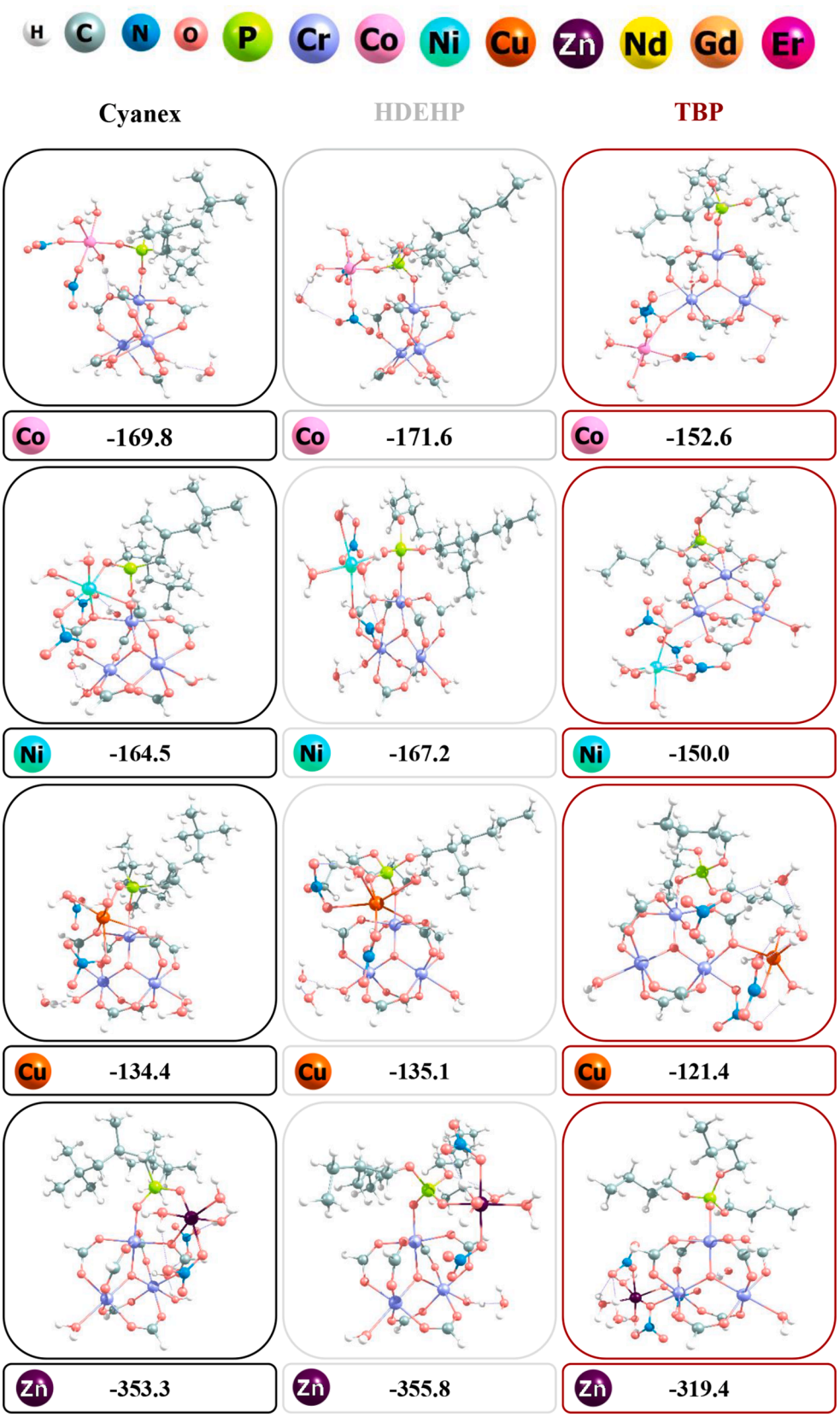


**Fig. 4.** The global minimum structures of the OPC/MIL-101(Cr) model-metal ion ($M^{n+}$)-water-nitrate complexes obtained from GFN-xTB calculations in aqueous phase. The black, grey, and dark red panels respectively refer to Cyanex, HDEHP and TBP. The values written under each panel are the corresponding average complexation Gibbs free energies in kJ $mol^{-1}$ at 1 atm and 298.15 K.

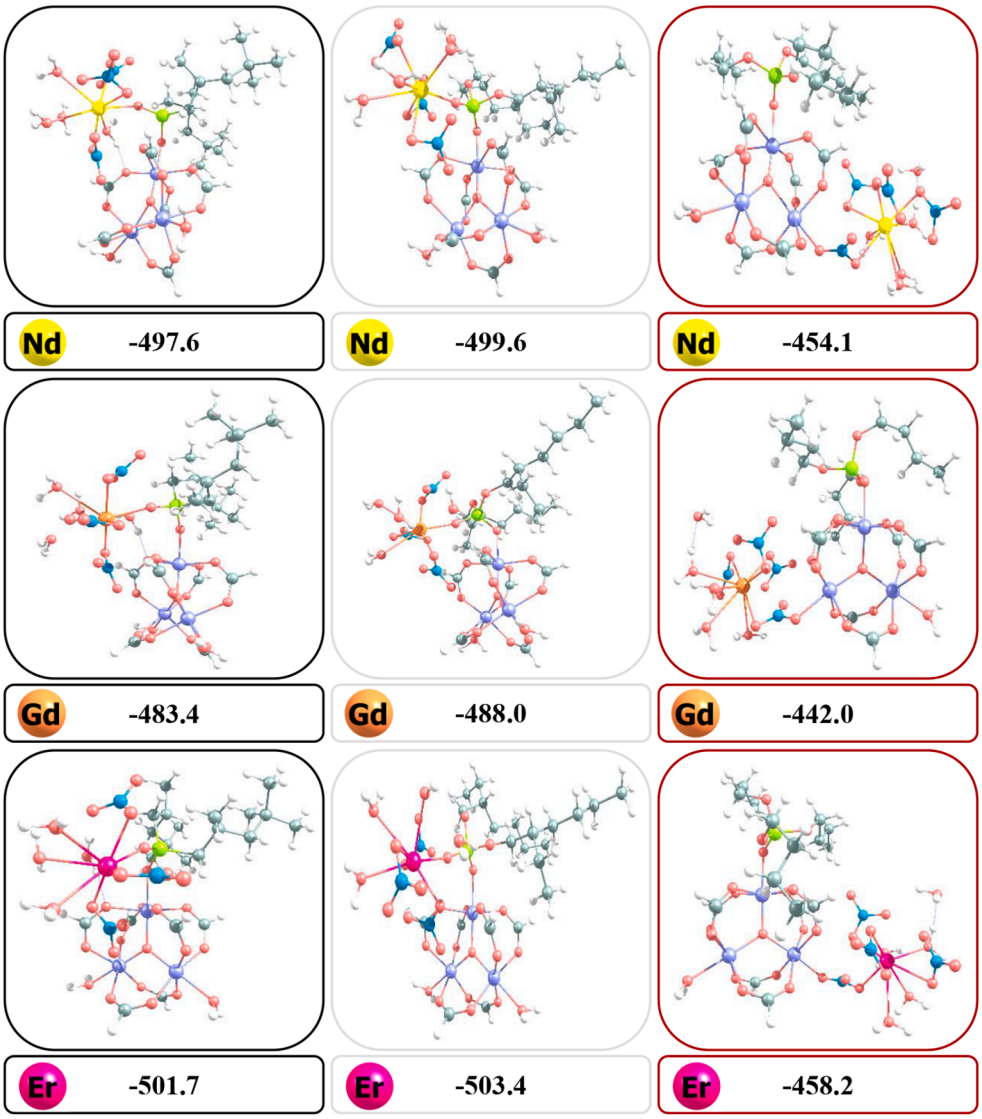


**Fig. 4.** (*continued*).

energy results reported in Table S7 and Fig. 4 clearly distinguish the performance of the MOFs in recovery of the REEs compared to the divalent metal ions. They also show higher efficiency for the HDEHP (and then Cyanex) containing MOFs in adsorbing the REEs and divalent metal ions compared to the TBP-grafted MIL-101(Cr) model. This is consistent with the $Er^{3+}$ adsorption capacities reported in our experimental work at pH 5.5 [10]: MIL-101-H50 (57.5 mg $g^{-1}$) > MIL-101-C50 (48.9 mg $g^{-1}$) > MIL-101-T50 (37.2 mg $g^{-1}$).

Furthermore, our results for all OPCs indicated that the tendency of the MOF in adsorptive recovery of the metal ions follows the order $Er^{3+}$ > $Nd^{3+}$ > $Gd^{3+}$ ≫ $Zn^{2+}$ ≫ $Co^{2+}$ > $Ni^{2+}$ > $Cu^{2+}$. In line with the obtained order, our experimental results of a mixture of $Er^{3+}$, $M^{2+}$ ions, and the Cyanex, HDEHP and TBP-modified samples outlined 91%, 96% and 100% selectivity towards $Er^{3+}$ and only 9%, 3% and 0% for $Zn^{2+}$, respectively [10]. Almost no adsorption of $Co^{2+}$, $Ni^{2+}$ or $Cu^{2+}$ was observed, in our experiments. Therefore, the overall computational order of metal adsorption and the large difference between the average complexation Gibbs free energies of the divalent and trivalent metals agree well with the experimental selectivity results.

The computational and experimental results outline two questions: "Why are the OPC-modified MOFs highly selective towards REE adsorption?" and "How does the change of the applied OPC alter the selectivity results?" To answer these, we should first point out that, according to our experiments [10], MIL-101(Cr) cannot adsorb the REEs significantly meaning that the exceptional adsorption of the trivalent ions is a consequence of OPC grafting onto the SBUs of the framework. As OPCs cap the metal node (making the Cr-sites inaccessible by the ions), this implies that the phenyl-containing ligands of MIL-101(Cr) do not contribute significantly to metal recovery. The hypothesis was justified by adopting the HDEHP-b/MIL-101(Cr) model shown in Fig. 3 and repeating the configurational sampling process for $Er^{3+}$ recovery, as a sample system. Comparison of the $Er^{3+}$ recovery modes of the ligand-free and ligand-containing models (Fig. S7) clarifies the importance of OPC-binding and lack of any direct interaction between the hydrated and nitrated metal ion and the MOF's ligands.

Further, as shown in Fig. 4, metal ion recovery by the MOF models follows two general complexation modes. In the first mode, observed for the HDEHP and Cyanex containing systems, the metal ion is bound to the Cr-free oxygen atom of the OPCs. The metal ion can be as well connected to the SBU's neighboring oxygen atom or the oxygen atom of a nitrate anion, highlighting the importance of electrostatic interactions. As the REEs carry more positive charge (compared to the divalent metal ions), they show a higher affinity towards the negatively charged MOF atoms with localized electron density, facilitating charge transfer between the metal ion-MOF pairs. For $Zn^{2+}$, its higher ionic radius and lower electronegativity relative to other divalent metal ions (see Table S7) increase

its tendency towards stabilization by π-bonding between the *d*-orbitals of Zn and the lone pair electrons of the bridging oxygen atoms.

The second complexation mode is only observed for TBP/MIL-101 (Cr). In this mode, the metal ions are complexed to a nitrate ion which binds to the Cr atom of the SBU far from TBP. As an interesting outcome, TBP cannot directly contribute to stabilization of the metal ions and the net metal ion-MOF binding energy increases (i.e., metal ion-MOF binding weakens). However, TBP can alter the extent of $Er^{3+}$ recovery by changing the charge distribution of the SBU in MIL-101(Cr) and promoting the selective uptake of $Er^{3+}$ from mixed solutions by MIL-101-T50.

In general, the instability of TBP-SBU interaction in aqueous solutions (Section 3.2) and its unique metal ion binding mode diminish the performance of TBP/MIL-101(Cr) in metal recovery (37.2 mg $g^{-1}$ maximum $Er^{3+}$ uptake vs. 48.9 mg $g^{-1}$ for Cyanex and 57.5 mg $g^{-1}$ for HDEHP) [10]. The higher $Er^{3+}$ uptake by HDEHP cannot be solely explained by the binding modes since the binding modes of HDEHP and Cyanex are similar. However, the binding modes and accessibility of the binding sites can be relevant. The decrease of the specific surface area of MIL-101(Cr) caused by the addition of the OPCs (see Section 3.1) can affect the diffusion of the REE ions and, thus, their binding to the adsorption sites.

Another reason for the high selectivity of the MOFs towards REEs can be associated with their high polarizabilities (and charge-to-radius ratios) (see Table S7), facilitating their hydration and coordination with nitrate anions. It is evident in Fig. 4 that all metal ions are hydrated and/or contain nitrate anions in their coordination shells and the water and nitrate molecules play a crucial role in their binding to the MOFs. Therefore, any future study simulating metal ion uptake and recovery from aqueous solutions should concern the presence of explicit water molecules and important ions.

The modelling results also show higher affinity towards $Er^{3+}$ from a solution of mixed REEs ($Er^{3+}$, $Gd^{3+}$ and $Nd^{3+}$). This is consistent with the experimental distribution coefficients and separation factors reported in our experimental work and Table S8 [10]. However, our calculations fail to reproduce the higher tendency of the three OPC-grafted MOFs towards $Gd^{3+}$ (relative to $Nd^{3+}$) and consequently they cannot explain the 95%, 5% and 0% selectivity of the TBP-modified MOF towards $Er^{3+}$, $Gd^{3+}$ and $Nd^{3+}$, respectively [10]. The reason can be related to the level of approximations implemented in the GFN2-xTB semi-empirical calculations. The studied REEs are *f*-elements and their *f*-orbitals can contribute to their functionalities. However, GFN2-xTB calculations approximate the contribution of the *f*-orbitals as "*f*-in-core" pseudo-potentials, and utilize global empirical parameters linearly interpolated with nuclear charge for Nd, Gd and Er [75]. Another approximation that might have affected the quantitative results is the application of fractional orbital occupation (or the Fermi-smearing technique) in measuring dynamical and static electron correlation, decreasing the accuracy of complexation energies [78]. Therefore, we expect the limitation of our calculations to be resolved by performing higher level DFT calculations. Also, we expect that the addition of all mixture metal ions to the configurationally sampled system instead of considering one metal ion at a time can partially neutralize the effect of approximations on the relative energies. Furthermore, such approach permits studying the involved cooperative/competitive adsorption processes. However, both solutions increase the computational cost drastically and prevent intensive high-level calculations. Based on the results, the GFN2-xTB calculations should suffice in depicting a general mechanistic picture of metal recovery from aqueous solutions.

Despite the approximations, we believe that the higher affinity of the MOFs towards $Er^{3+}$ (and then $Gd^{3+}$) is related to their specific electron configuration as 4*f*-elements. The difference in the inter-electron repulsion energies of 4*f* electrons within lanthanide series affects their stabilization energies and coordination chemistry [79,80]. Their coordination number decreases with their ionic radii from $Nd^{3+}$ to $Gd^{3+}$ and $Er^{3+}$ [81,82], as their charge-to-radius ratios increase because of lanthanide contraction. As an outcome, the heavier REEs present a higher potency of uptake by the modified MOFs.

Lastly, the experimental results demonstrated the highest selectivity towards heavier REEs for TBP/MIL-101 (followed by HDEHP/MIL-101) though its adsorption affinity is the lowest (see Table S8) [10]. The reason is related to the metal uptake configurations shown in Fig. 4 and the Hard-Soft-Acid-Base (HSAB) theory [83]. As the complexation mode of the REE ions relies on the bridge formed via the oxygen atoms of the SBU or the OPCs, the selectivity order $Nd^{3+} < Gd^{3+} < Er^{3+}$ follows the HSAB principle – the softer the base group (HDEHP < Cyanex), the lower the selectivity for coordination with heavier REEs (due to an increase in charge density and Lewis acid strength) [84].

## 4. Conclusion

The present computational study proposes an efficient modeling approach to unravel the mechanistic processes controlling highly selective recovery of REEs from aqueous solutions by OPC-modified MIL-101(Cr). Our most important findings, summarized here, will guide further material development and separation studies. Our DFT calculations show that any environmental factor affecting the bond formed between the oxygen of OPC and the Cr atom of the MOF can affect the stability and performance of the synthesized MOF. However, the alkyl groups of the OPCs do not significantly affect the corresponding interactions, unless their nature influences the charge accumulated on the OPC's oxygen atoms. As the O(OPC)-Cr(MOF) bond plays a central role in the chemistry of the process, further studies are encouraged to evaluate the changes in the strength of the bond using similar computational methods or (a combination of) experimental spectroscopies, such as FT-IR, Raman and X-ray photoelectron (XPS). Our results also indicate that stronger adsorption of Cyanex-272 and HDEHP onto MIL-101(Cr) increases the stability of Cyanex-272/MIL-101(Cr) and HDEHP/MIL-101 (Cr) relative to TBP/MIL-101(Cr). Furthermore, our modelling reveals that the decrease in the available surface area after grafting the OPCs onto MIL-101(Cr) is caused by their umbrella-like configuration inside the MOF pores. This can also contribute to the lower adsorption of $Er^{3+}$ and slower kinetics of Cyanex-272/MIL-101 relative to HDEHP/MIL-101, observed in our experimental studies. We have also noticed lower chemical stability for TBP/MIL-101(Cr) and a rather unique metal uptake mode, leading to lower efficiency in metal recovery but remarkably higher selectivity towards $Er^{3+}$. Moreover, we found the key binding mode for improved REE recovery and selectivity to be the mode in which the target metal ion binds to the oxygen of the OPCs. The selectivity principle is based on the intrinsic ionic properties of the *f*-elements. Clearly, our computational method can showcase high selectivity of the OPC-modified MOFs towards REEs and their low tendency towards divalent metal ions. However, the method can be further improved by including cooperative/competitive metal adsorption and higher level first principles calculations. Finally, as all metal ions were found hydrated and/or coordinated to nitrate anions in the most stable $M^{n+}$/MOF/nitrate/water complexes, and the coordinated water and nitrate molecules play a crucial role in metal ion binding to the MOFs, any modelling study of metal ion uptake and recovery from aqueous solutions should consider explicit water molecules and important counterions.

## Declaration of Competing Interest

The authors declare that they have no known competing financial interests or personal relationships that could have appeared to influence the work reported in this paper.

## Acknowledgements

We appreciate financial support by Academy of Finland (Grant no. 330076 and 336423), the Emil Aaltonen Foundation (Grant no. 180288)

and the Walter Ahlström Foundation. We also acknowledge the CSC-IT Center for Science (Finland) for provision of computational resources.

## Appendix A. Supplementary data

Details about spin state selection (Section S1; Tables S1 and S2 and Figs. S1-S3), the choice of the optimal computational level (Section S2; Table S3), optimized geometries of the organophosphorus compounds (OPCs) and the OPC-grafted MOF models in water, toluene and gas phases (Figs. S4 and S5), the grafting thermodynamics, NBO results and metal uptake results (Tables S4-S7 and Fig. S7) and the summary of the important experimental data including BET surface areas (Fig. S5), and metal separation factors (Table S8). All optimized structures would be freely provided upon request. Supplementary data to this article can be found online at https://doi.org/10.1016/j.cej.2022.135905.

## References


[1] B. Swain, E.O. Out, Sep. Purif. Technol. 83 (2011) 82–90.
[2] C. Gropp, S. Canossa, S. Wuttke, F. Gándara, Q. Li, L. Gagliardi, O.M. Yaghi, A.C. S. Cent, Sci. 6 (2020) 1255–1273.
[3] Y. Zhao, Chem. Mater. 28 (2016) 8079–8081.
[4] M.J. Kalmutzki, C.S. Diercks, O.M. Yaghi, Adv. Mater. 30 (2018) 1704304.
[5] S. Yuan, J.-S. Qin, C.T. Lollar, H.-C. Zhou, A.C.S. Cent, Sci. 4 (2018) 440–450.
[6] C. Wang, X. Liu, N. Keser Demir, J.P. Chen, K. Li, Chem. Soc. Rev. 45 (2016) 5107–5134.
[7] Y. Sun, L. Zheng, Y. Yang, X. Qian, T. Fu, X. Li, Z. Yang, H. Yan, C. Cui, W. Tan, Nano Micro Lett. 12 (2020) 1–29.
[8] S. Li, Y. Chen, X. Pei, S. Zhang, X. Feng, J. Zhou, B. Wang, Chin. J. Chem. 34 (2016) 175–185.
[9] P.A. Kobielska, A.J. Howarth, O.K. Farha, S. Nayak, Coord. Chem. Rev. 358 (2018) 92–107.
[10] V. Kavun, M.A. van der Veen, E. Repo, Micropor. Mesopor. Mat. 312 (2021) 110747–110755.
[11] Y. Hu, J. Florek, D. Larivière, F.-G. Fontaine, F. Kleitz, Chem. Rec. 18 (2018) 1261–1276.
[12] A.F. Wells, Structural inorganic chemistry, Oxford University Press, 2012.
[13] F. Xie, T.A. Zhang, D. Dreisinger, F. Doyle, Miner. Eng. 56 (2014) 10–28.
[14] M.K. Jha, A. Kumari, R. Panda, J.R. Kumar, K. Yoo, J.Y. Lee, 165 (2016) 2-26.
[15] A. Battsengel, A. Batnasan, K. Haga, A. Shibayama, J. Miner. Mater. Charact. Eng. 6 (2018) 517–530.
[16] C. Basualto, J. Gaete, L. Molina, F. Valenzuela, C. Yañez, J.F. Marco, Sci. Techol. Adv. Mater. 16 (2015), 035010.
[17] M.S. Gasser, E. El Sherif, R.O. Abdel Rahman, Chem. Eng. J. 316 (2017) 758–769.
[18] Z. Hualei, L.I. Dongyan, T. Yajun, C.H.E.N. Yunfa, Rare Met. 27 (3) (2008) 223–227.
[19] Q. Shu, A. Khayambashi, Q. Zou, X. Wang, Y. Wei, L. He, F. Tang, J. Radioanal. Nucl. Chem. 313 (2017) 29–37.
[20] X. Hérès, V. Blet, P. di Natale, A. Ouaattou, H. Mazouz, D. Dhiba, F. Cuer, Metals 8 (2018) 682.
[21] J. Veliscek-Carolan, T.L. Hanley, V. Luca, Sep. Purif. Technol. 129 (2014) 150–158.
[22] V. Luca, J.J. Tejada, D. Vega, G. Arrachart, C. Rey, Inorg. Chem. 55 (2016) 7928–7943.
[23] M. Zhang, K. Yang, J. Cui, H. Yu, Y. Wang, W. Shan, Z. Lou, Y. Xiong, Chem. Eng. J. 386 (2020), 124023.
[24] I. Ahmed, K.K. Adhikary, Y.R. Lee, K.H. Row, K.K. Kang, W.S. Ahn, Chem. Eng. J. 370 (2019) 792–799.
[25] A.F. Abdel-Magied, H.N. Abdelhamid, R.M. Ashour, X. Zou, K. Forsberg, Micropor. Mesopor. Mat. 278 (2019) 175–184.
[26] F. Zhao, E. Repo, Y. Song, D. Yin, S.B. Hammouda, L. Chen, S. Kalliola, J. Tang, K. C. Tam, M. Sillanpää, Green Chem. 19 (2017) 4816–4828.
[27] Y. Hu, E. Drouin, D. Larivière, F. Kleitz, F.G. Fontaine, A.C.S. Appl, Mater. Interfaces 9 (2017) 38584–38593.
[28] J. Wu, Z. Li, H. Tan, S. Du, T. Liu, Y. Yuan, X. Liu, H. Qiu, Anal. Chem. 93 (2020) 1732–1739.
[29] J. Florek, D. Larivière, H. Kählig, S.L. Fiorilli, B. Onida, F.-G. Fontaine, F. Kleitz, A. C.S. Appl, Mater. Interfaces 12 (2020) 57003–57016.
[30] S.M. Ibrahim, Y. Zhang, Y. Xue, S. Yang, F. Ma, Y. Gao, Y. Zhou, G. Tian, ACS Omega 4 (2019) 20797–20806.
[31] N.K. Batchu, Z. Li, B. Verbelen, K. Binnemans, Sep. Purif. Technol. 255 (2021), 117711.
[32] A.D. Braatz, M.R. Antonio, M. Nilsson, Dalton Trans. 46 (2017) 1194–1206.
[33] J. Luo, C. Wang, J. Lan, Q. Wu, Y. Zhao, Z. Chai, C. Nie, W. Shi, Sci. China Chem. 59 (2016) 324–331.
[34] M.J. Frisch, G.W. Trucks, H.B. Schlegel, G.E. Scuseria, M.A. Robb, J.R. Cheeseman, G. Scalmani, V. Barone, G.A. Petersson, H. Nakatsuji, et al., Gaussian 16 Revision A.03, Gaussian, Inc., Wallingford CT, 2016.
[35] A. Mavrandonakis, K.D. Vogiatzis, A.D. Boese, K. Fink, T. Heine, W. Klopper, Inorg. Chem. 54 (2015) 8251–8263.
[36] A. de Oliveira, A. Mavrandonakis, G.F. de Lima, H.A. de Abreu, ChemistrySelect 2 (2017) 7813–7820.
[37] T.-D. Hu, Y.-W. Sun, Y.-H. Ding, J. CO2 Util. 28 (2018) 200–206.
[38] A. Pourreza, S. Askari, A. Rashidi, A. Seif, M. Kooti, Chem. Eng. J. 363 (2019) 73–83.
[39] M. Barona, R.Q. Snurr, A.C.S. Appl, Mater. Interfaces 12 (2020) 28217–28231.
[40] Q.-X. Luo, M. Ji, M.-H. Lu, C. Hao, J.-S. Qiu, Y.-Q. Li, J. Mater. Chem. A 1 (2013) 6530–6534.
[41] J. Kim, T.K. Kim, J. Kim, Y.S. Lee, H. Ihee, J. Phys. Chem. A 111 (2007) 4697–4710.
[42] S.J. Stoneburner, L. Gagliardi, J. Phys. Chem. C 122 (2018) 22345–22351.
[43] J.G. Vitillo, E. Groppo, S. Bordiga, S. Chavan, G. Ricchiardi, A. Zecchina, Inorg. Chem. 48 (2009) 5439–5448.
[44] A.D. Becke, J. Chem. Phys. 98 (1993) 5648–5652.
[45] Y. Zhao, D.G. Truhlar, Theor. Chem. Acc. 120 (2008) 215–241.
[46] J.P. Perdew, K. Burke, M. Ernzerhof, Phys. Rev. Lett. 77 (1996) 3865–3868.
[47] K. Burke, J.P. Perdew, Y. Wang, Electronic density functional theory: recent progress and new directions, Springer Science & Business Media, 2013.
[48] J.-D. Chai, M. Head-Gordon, Phys. Chem. Chem. Phys. 10 (2008) 6615–6620.
[49] J.-W. Shin, M. Kim, J. Cirera, S. Chen, G.J. Halder, T.A. Yersak, F. Paesani, S. M. Cohen, Y.S. Meng, J. Mater. Chem. A 3 (2015) 4738–4744.
[50] K.D. Vogiatzis, W. Klopper, A. Mavrandonakis, K. Fink, ChemPhysChem 12 (2011) 3307.
[51] S. Abdpour, E. Kowsari, B. Bazri, M.R. Alavi Moghaddam, S. Sarabadani Tafreshi, N.H. de Leeuw, I. Simon, L. Schmolke, D. Dietrich, S. Ramakrishna, C. Janiak, J. Mol. Liq. 319 (2020), 114341.
[52] L. Kollias, D. Cantu, V.-A. Glezakou, R. Rousseau, M. Salvalaglio, Adv. Theory Simul. 3 (2020) 2000092.
[53] X.-J. Hou, H. Li, P. He, Comput, Theor. Chem. 1055 (2015) 8–14.
[54] K. Liu, S. Zhang, X. Hu, K. Zhang, A. Roy, G. Yu, Environ. Sci. Tech. 49 (2015) 8657–8665.
[55] J. Toda, M. Fischer, M. Jorge, J.R.B. Gomes, Chem. Phys. Lett. 587 (2013) 7–13.
[56] S. Grimme, J. Antony, S. Ehrlich, H. Krieg, J. Chem. Phys. 132 (2010) 154104–154119.
[57] F. Weigend, F. Ahlrichs, Phys. Chem. Chem. Phys. 7 (2005) 3297–3305.
[58] F. Weigend, Phys. Chem. Chem. Phys. 8 (2006) 1057–1065.
[59] J.M. Voss, B.M. Marsh, J. Zhou, E. Garand, Phys. Chem. Chem. Phys. 18 (2016) 18905–18913.
[60] A.V. Marenich, C.J. Cramer, D.G. Truhlar, J. Phys. Chem. B 113 (2009) 6378–6396.
[61] J. Kubečka, V. Besel, T. Kurtén, N. Myllys, H. Vehkamäki, J. Phys. Chem. A 123 (2019) 6022–6033.
[62] F. Keshavarz, T. Kurtén, H. Vehkamäki, J. Kangasluoma, J. Phys. Chem. A 124 (2020) 10527–10539.
[63] K.K. Dingilian, M. Lippe, J. Kubečka, J. Krohn, C. Li, R. Halonen, F. Keshavarz, B. Reischl, T. Kurtén, H. Vehkamäki, R. Signorell, J. Phys. Chem. Lett. 12 (2021) 4593–4599.
[64] F. Keshavarz, J. Kubecka, M. Attoui, H. Vehkamaki, T. Kurten, J. Kangasluoma, J. Phys. Chem. C 124 (2020) 26944–26952.
[65] F. Keshavarz, J.A. Thornton, H. Vehkamäki, T. Kurtén, ACS Earth Space Chem. 5 (2021) 210–225.
[66] F. Keshavarz, New J. Chem. 45 (2021) 6709–6723.
[67] A.M. Wilson, P.J. Bailey, P.A. Tasker, J.R. Turkington, R.A. Grant, J.B. Love, Chem. Soc. Rev. 43 (2014) 123–134.
[68] J. Zhang, M. Dolg, Phys. Chem. Chem. Phys. 17 (2015) 24173–24181.
[69] J. Zhang, M. Dolg, Phys. Chem. Chem. Phys. 18 (2016) 3003–3010.
[70] M.C. Bernini, D. Fairen-Jimenez, M. Pasinetti, A.J. Ramirez-Pastor, R.Q. Snurr, J. Mater. Chem. B 2 (2014) 766–774.
[71] A. Das, S.M. Ali, J. Chem. Phy. 148 (2018) 074502–074514.
[72] V. Migliorati, A. Serva, F.M. Terenzio, P. D'Angelo, Inorg. Chem. 56 (2017) 6214–6224.
[73] P. Li, K.M. Merz Jr., J. Chem. Theory Comput. 10 (2014) 289–297.
[74] S. Grimme, C. Bannwarth, P. Shushkov, J. Comput. Theory Chem. 13 (2017) 1989–2009.
[75] C. Bannwarth, S. Ehlert, S. Grimme, J. Chem. Theory Comput. 15 (2019) 1652–1671.
[76] S. Ehlert, M. Stahn, S. Spicher, S. Grimme, A robust and efficient implicit solvation model for fast semiempirical methods (2021), https://doi.org/10.26434/chemrxiv.14555355.v1.
[77] G. Sigalov, A. Fenley, A. Onufriev, J. Chem. Phys. 124 (2006) 124902–124914.
[78] S. Grimme, A. Hansen, Angew. Chem. Int. Ed. 54 (2015) 12308–12313.
[79] S. Andersson, K. Eberhardt, C. Ekberg, J.-O. Liljenzin, M. Nilsson, G. Skarnemark, Radiochim. Acta 94 (2006) 469–474.
[80] M. Dobler, P. Guilbaud, A. Dedieu, G. Wipff, New J. Chem. 25 (2001) 1458–1465.
[81] S. Alizadeh, M. Abdollahy, A. Khodadadi Darban, M. Mohseni, J. Mol. Liq. 333 (2021), 116015.
[82] W.W. Rudolph, G. Irmer, J. Solution Chem. 49 (2020) 316–331.
[83] R.G. Pearson, J. Am. Chem. Soc. 85 (1963) 3533–3539.
[84] M. Gergoric, C. Ekberg, B.-M. Steenari, T. Retegan, J. Sustain. Met. 3 (2017) 601–610.